

Numerical Exploration of Soliton Creation

Henry Lamm, Tanmay Vachaspati

Physics Department, Arizona State University, Tempe, AZ 85287

We explore the classical production of solitons in the easy axis $O(3)$ model in 1+1 dimensions, for a wide range of initial conditions that correspond to the scattering of small breathers. We characterize the fractal nature of the region in parameter space that leads to soliton production and find certain trends in the data. We identify a tension in the initial conditions required for soliton production – low velocity incoming breathers are more likely to produce solitons, while high velocity incoming breathers provide momentum to the final solitons and enable them to separate. We find new “counter-spinning” initial conditions that can alleviate some of this tension.

I. INTRODUCTION

Perturbative field theory is an expansion around a single vacuum state but many field theories admit multiple degenerate vacua. Excitations in such field theories include solitons that interpolate between different vacua in addition to the particle excitations around a single vacuum. While solitons and particles are distinct excitations, it is generally possible to transition from one to the other. For example, a soliton and anti-soliton are able to annihilate and produce particles. Here we shall be concerned with the reverse process in which we start with particles and create a soliton-antisoliton pair.

The transition from particles to solitons (or vice versa) has another layer of complexity because it is also a transition from a quantum system (particles) to a classical system (solitons). A rigorous formalism to treat the transition is not known. While some attempts have been made at semiclassical and quantum calculations [1–8], the most straightforward approach at the current time is to treat the entire process classically. Particles in the initial state are replaced by classical field configurations that are non-dissipative, like “breathers” of the sine-Gordon model [9], or dissipative but long-lived, like “oscillons” [10–12] in other models.

Previous work on the classical production of solitons has mostly been carried out in the $\lambda\phi^4$ model, which has the virtue that it has the minimal structure necessary for studying the process [10, 11, 13, 14]. However, the simplicity of the model may also be a drawback, as additional degrees of freedom [9] or a more complex potential [8, 12] may facilitate the production of solitons. Thus we study soliton production in the easy axis $O(3)$ model (described in detail in Sec. II).

The easy axis $O(3)$ model (or “ $O(3)_z$ model”) in 1+1 dimensions has a number of features that make it suitable for studying soliton production. As the model has two degenerate vacua, it contains kink solutions. Certain subspaces of the model are equivalent to the classical sine-Gordon model. Thus the model also has breather solutions that do not decay and can be used to mimic incoming particle states. The $O(3)_z$ model has an additional “twist” degree of freedom that gives it more complexity than the $\lambda\phi^4$ model and brings it a bit closer to models with ‘t Hooft-Polyakov magnetic monopoles, as monopoles also carry a phase degree of freedom.

This paper is organized as follows. In Sec. II we describe the $O(3)_z$ model and in Sec. III we describe the range of initial conditions that we use in our scattering simulations. Our numerical results are discussed in Sec. IV and we conclude in Sec. V.

II. EASY AXIS $O(3)$ MODEL

The $O(3)_z$ model in 1+1 dimensions is given by the action

$$S = \int d^2x \left[\frac{1}{2}(\partial_\mu \mathbf{n})^2 - \frac{1}{2}(1 - n_3^2) - \lambda(\mathbf{n}^2 - 1) \right] \quad (1)$$

where $\mathbf{n}(t, x)$ is a vector field with Cartesian components (n_1, n_2, n_3) and λ is a Lagrange multiplier that forces \mathbf{n} to have unit magnitude: $\mathbf{n}^2 = 1$. The potential term reduces the $O(3)$ symmetry to $O(2) \times Z_2$, corresponding to symmetry under rotations in the n_1 - n_2 plane and to reflections of n_3 . There are two degenerate vacua: $\mathbf{n} = (0, 0, \pm 1)$.

After eliminating the constraint condition, the equation of motion is

$$\square \mathbf{n} + (\partial_\mu \mathbf{n})^2 \mathbf{n} - n_3(\hat{e}_3 - n_3 \mathbf{n}) = 0, \quad \mathbf{n}^2 = 1 \quad (2)$$

where $\hat{e}_3 \equiv (0, 0, 1)$.

Alternately, the constraint can be solved explicitly in terms of angular variables, $\mathbf{n} = (\sin \theta \cos \phi, \sin \theta \sin \phi, \cos \theta)$, to give the action

$$S = \int d^2x \left[\frac{1}{2} (\partial_\mu \theta)^2 + \frac{1}{2} \sin^2 \theta (\partial_\mu \phi)^2 - \frac{1}{2} \sin^2 \theta \right] \quad (3)$$

which leads to the equations of motion

$$\square \theta + \sin \theta \cos \theta (1 - (\partial_\mu \phi)^2) = 0 \quad (4)$$

$$\partial_\mu (\sin^2 \theta \partial^\mu \phi) = 0. \quad (5)$$

The latter equation is of the form $\partial_\mu j^\mu = 0$ and so $j^0 = \sin^2 \theta \dot{\phi}$ is the charge density of a conserved current in the model.

Let $\alpha \equiv 2\theta$ and consider the case, $\phi = \text{constant}$. Then the equation of motion reduces to

$$\square \alpha + \sin \alpha = 0 \quad (6)$$

which is identical to the equation of motion for the sine-Gordon model. (This can also be seen at the level of the action.) Hence the $O(3)_z$ model inherits all the solutions of the sine-Gordon model. In particular

$$\theta_k(x) = 2 \tan^{-1}(e^x), \quad \phi = \text{constant} \quad (7)$$

is a kink solution in which \mathbf{n} is at the North pole in field space at $x = -\infty$ and at the South pole at $x = +\infty$. With our normalization, the energy of the kink is $E_k = 2$. The model also inherits the (boosted) sine-Gordon breather solutions

$$\theta_b(x, t) = 2 \tan^{-1} \left[\frac{\eta \sin(\omega T)}{\cosh(\eta \omega X)} \right], \quad \phi = \text{constant} \quad (8)$$

where

$$T = \gamma(t - v(x - x_0)) \quad (9)$$

$$X = \gamma((x - x_0) - vt). \quad (10)$$

The parameter x_0 is the initial position of the breather, v its velocity, and $\gamma = 1/\sqrt{1 - v^2}$ its Lorentz factor. The parameter ω is the oscillation frequency of the breather and takes values in $[0, 1]$, while η is defined by

$$\eta = \sqrt{1 - \omega^2}/\omega \quad (11)$$

The typical waveform of a boosted breather can be seen in Fig. 1.

The energy in a field configuration is given by

$$E = \int dx H(t, x) = \int dx \left[\frac{\dot{\theta}^2}{2} + \frac{\theta'^2}{2} + \sin^2 \theta \frac{\dot{\phi}^2}{2} + \sin^2 \theta \frac{\phi'^2}{2} + \frac{1}{2} \sin^2 \theta \right] \quad (12)$$

For a boosted breather, the energy evaluates to

$$E_b = 4\gamma \sqrt{1 - \omega^2} = 4\gamma \eta \omega \quad (13)$$

and the rest mass of the breather is

$$m_b = \frac{E_b}{\gamma} = 4\sqrt{1 - \omega^2} = 4\eta \omega \quad (14)$$

Note that the energy of the breather is smaller for larger ω and vanishes for $\omega = 1$. If we choose initial conditions on a great circle ($\phi = \phi_0, \phi_0 + \pi$), the dynamics will also be restricted to the great circle. Then the evolution is exactly as in the sine-Gordon model. As the sine-Gordon model is completely integrable [15], both the number of kinks and the number of anti-kinks are conserved and we can not create kinks (or antikinks) if there were none in the initial conditions. Hence it is crucial to choose initial conditions in which ϕ is not a constant *i.e.* that the initial conditions be “twisted” in the ϕ direction.

A general feature in 1+1 classical field theory of interest to us will be that the interaction force between two static solitons separated by a distance L is proportional to

$$F(L) \propto e^{-L/a} \quad (15)$$

where a is a length scale, usually on the order of the width of a soliton [16].

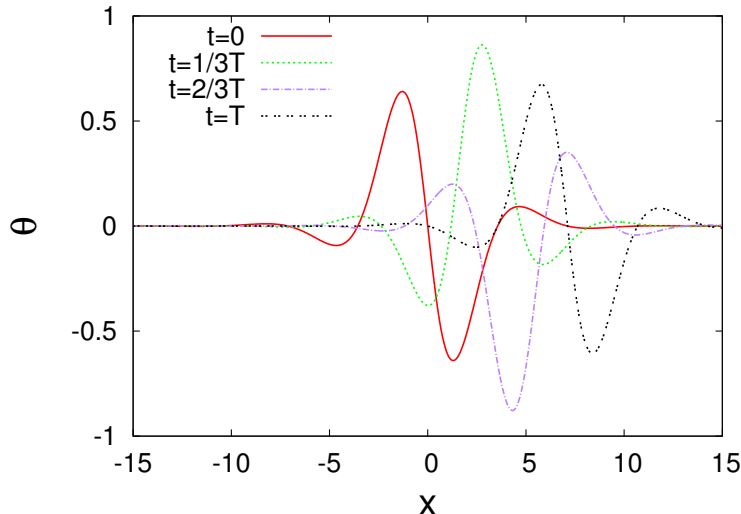


FIG. 1: Field profile (θ) of a boosted breather at different times over an oscillation period. The particular parameters used are $v = 0.9$, $\omega = 0.90$ which corresponds to $m_b = 1.74$.

III. CHOICE OF INITIAL CONDITIONS

Ideally we would like to start with initial conditions that describe incoming particles in some energy range, but then the initial condition would have to be described in terms of quantum field theory. On the other hand, the final state of interest has kinks, and these are classical objects. So the creation of kinks from particles also involves a transition from an initial quantum system to a final system that contains classical elements, and a formalism to describe such a transition is not known. The simplification we will adopt is to consider initial conditions that only contain breathers as, at least in the sine-Gordon model, it has been shown that quantized breathers correspond to particles of the theory in the low mass limit [17].

Our choice of initial conditions consists of a train of N left-moving breathers and N right-moving breathers. The parameters m_b and v characterize an individual breather in the train. In addition, we can vary the spacing of the breathers within a train, the number of breathers in each train, and the relative twists of the breathers. This last parameter is called ξ and is defined by

$$\xi \equiv \frac{\phi_L - \phi_R}{2\pi} \quad (16)$$

where ϕ_L , ϕ_R are the initial constant values of ϕ for the left- and right-moving breathers. Explicitly, the initial condition is

$$\theta(t = 0, x) = \sum_{j=1}^N [\theta_b(t = 0, x; -x_j, +v) + \theta_b(t = 0, x; +x_j, -v)] \quad (17)$$

$$\phi(t = 0, x) = \pi\xi \tanh(x/w) \quad (18)$$

$$\dot{\theta}(t = 0, x) = \sum_{j=1}^N [\dot{\theta}_b(t = 0, x; -x_j, v) + \dot{\theta}_b(t = 0, x; +x_j, -v)] \quad (19)$$

$$\dot{\phi}(t = 0, x) = 0 \quad (20)$$

where θ_b is the breather profile defined in Eq. (8) and the initial position of the j^{th} breather given by

$$x_j = x_0 + (j - 1)a. \quad (21)$$

Here x_0 is the initial position of the innermost breather in the train and a is the spacing between the breathers in a train. In our numerical runs, the parameter a is chosen to be twice the width of a breather, $a = 2w = 4/(\gamma\eta\omega)$, and x_0 is chosen to be $4E_b w$ which is much larger than the width of the breathers investigated. In the bulk of our analysis, we start with $\dot{\phi} = 0$, but in Sec. IV F we will also describe some results with initial conditions $\dot{\phi}(t = 0, x) \neq 0$.

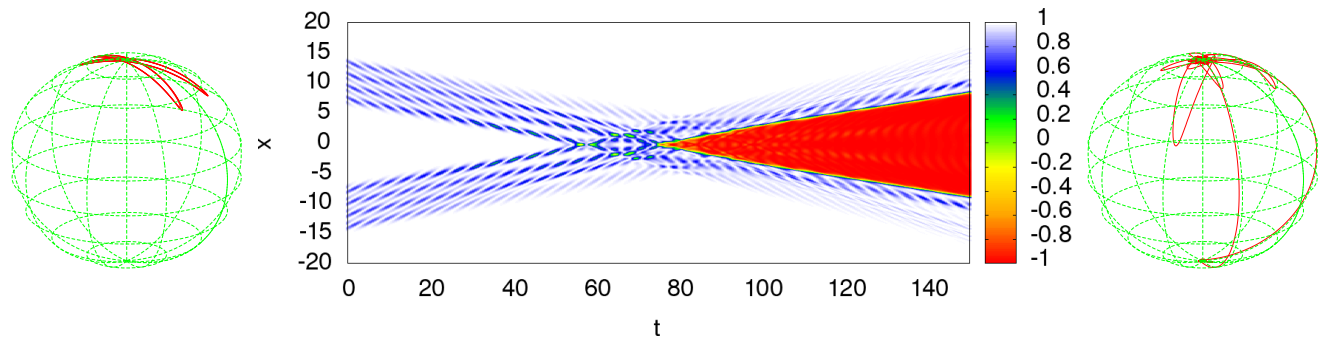


FIG. 2: The center panel indicates in color the n_3 field as a function of time (horizontal axis) and space measured in units of breather width (vertical axis) for the collision. Left and right panels are the vector field \mathbf{n} configurations at $t = 0$ and $t = 140$ respectively. The parameters for this scattering are $N = 4$, $m_b = 1.57$, $v_b = 0.55$, and $\xi = 0.1$. The final state contains a kink-antikink pair located at $x \approx \pm 6.4w$, where w is the width of the incoming breather.

The initial conditions listed above are used to construct the vector $\mathbf{n}(t = 0, x)$, which is then numerically evolved using Eq. (2). The numerical evolution is done using the explicit second order Crank-Nicholson method with two iterations [18].

We wish to explore a large number of initial conditions and to record only those initial conditions that lead to kink formation. Hence we need to specify criteria to decide if kinks were or were not produced in any given run. To do this, for each time step, we checked for a transition from $\cos \theta = 0$ to $\cos \theta = -0.99$. If this transition exists, the point where $\cos \theta = 0$ is considered to be the location of the kink at that time. By recording kink locations as a function of time, we were able to reconstruct the kink's path and therefore its velocity. To explore parameter space, we hold x_0 and a fixed and scan over a range of the 4 parameters: ω (breather frequency), v (incoming velocity), ξ (twist), and N (number of breathers in a train). To search this phase space for successful kink production, we used two different methods. For coarse grained searches, we used the MULTINEST software to find large clusters of conditions that lead to success [19, 20]. For fine grained searches at low mass, we scanned the initial conditions uniformly in steps of $\Delta v = 0.002$, $\Delta \xi = 0.001$ and $\Delta \omega = 0.01$. The ranges we explore are shown in Table I. We also show the corresponding range of the mass (m_b) and the Lorentz factor γ . (m_b and γ are derived from the ranges of ω and v .)

Parameter	Range
ω	0.500-0.990
v	0.100-0.990
ξ	0.000-0.500
N	1-20
m_b	0.565-3.500
γ	1.005-7.088

TABLE I: Range of initial conditions that we explore. For reference, the rest energy of a kink is 2.

We now describe our numerical results.

IV. NUMERICAL RESULTS

In Fig. 2 we show a sample event where a kink-antikink pair is produced. In the center we have the time evolution of the n_3 field. One should note that while the breathers are initially moving with the same velocity, interactions within a train change the separation and relative velocity between breathers. The importance of this effect will be discussed in Sec. IV E. The vector field $\mathbf{n}(t, x)$ is shown to the left and right of Fig. 2 at the initial and final times respectively.

We start by showing the cumulative result from all runs in the left panel of Fig. 3. Plotted is the number of successful kink production events versus the energy per incoming breather, after summing over all other parameters in the ranges shown in Table I. These results shows a peak in production when the energy of an individual breather

in the train is exactly the kink energy. This suggests that kink production is dominated by the collision of just two breathers scattering into a kink-antikink pair. However, we will show that multi-particle interactions within the train are critical to the success of these collisions and that having $E_b \approx 2$ is not a sufficient condition for kink production.

In the right panel of Fig. 3 we further partition the data of the left panel of Fig. 3 by the mass of the incoming breather but only for $N = 4$. In this plot we see that there is a distribution of energies for which kink production occurs, but the distribution is more narrowly distributed at smaller masses. In other words, if the incoming breather has small mass, it's energy must be picked more precisely. While the general distribution of energies seems to be smooth and peaked around $E_b = 2$, for a given mass of a breather there is a structure of clear peaks where success occurs, and a slight change in the energy can dramatically changes the success rate.

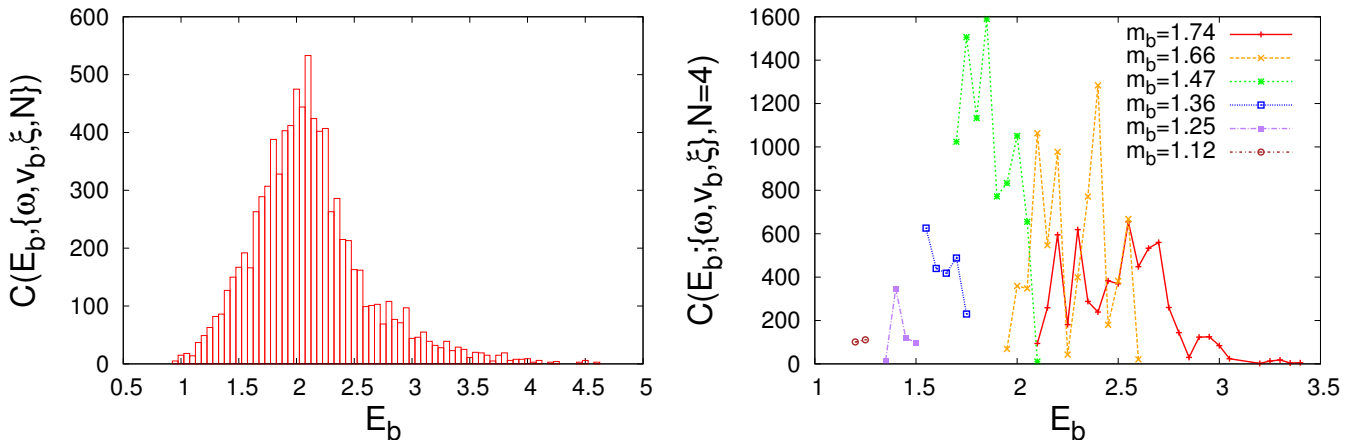


FIG. 3: Number of produced kinks vs. the energy of a single breather, summed over m_b, v_b, ξ, N for entire dataset. A strong peak is seen around the mass of a kink, $E_k = 2$. In the right-hand figure, we plot the number of produced kinks vs. energy of a single breather, split into groups by breather mass, summed over v_b, ξ but with $N = 4$.

Fig. 3 provides a summary of all our runs but loses information about the effects of varying parameters on kink production. In order to untangle some of these effects, we investigated the case of $N = 4$. This condition was chosen as a balance between the increased number of successes that comes from having larger N , and the simpler dynamics afforded by the few-body collisions of small N . For $N = 4$, we were able to find hundreds of successful initial conditions. From these results, we computed the velocity of the outgoing kinks as a function of the initial conditions. For three values of m_b , the outgoing kink velocities are plotted in Fig. 4.

A few distinct features can be seen in Fig. 4. With increasing breather mass, we see that the likelihood of producing kinks increases, but the range of velocities that yield kinks in the final state shift to higher values. Breather velocities where solitons are produced are found to form bands, reminiscent of [14] where the annihilation of solitons into particle-like states was considered. The chaotic results – note the hole at $v_b = 0.7, \xi = 0.1$ in the middle panel – also bear a qualitative resemblance to the production found in [11].

In these plots, the likelihood of kink production is suppressed in a region around $\xi \approx 0.25 - 0.35$ except at higher velocities where kink production is relatively insensitive to changes in twist. Another interesting feature is found by considering the dependence of clustering in the (m_b, v_b) plane. In Fig. 5, we plot the outgoing kink velocity for $\xi = 0.10$. Notice the counter-intuitive trend that for decreasing breather mass, m_b , successful kink production requires a *decrease* in the incoming velocity. This is the same dependence found in the $\lambda\phi^4$ model [10] and suggests a difficulty in the production of solitons from quantum particles as we will discuss below.

Also of interest in Fig. 5 is the appearance of two bands, one at high m_b and another at low m_b . Inside of each band, we see that increasing the breather mass requires an increase in velocity for kink production to be successful. The optimal velocity for kink production is a function of breather mass, and it increases within a band, but then has a large discontinuous jump as we cross from one band to another.

Next we focus on the kink velocity, v_k , in the runs that successfully produced a kink-antikink pair. Fig. 6 shows the dependence of v_k on the parameters m_b, v_b and ξ , where we fix $N = 4$. For example, the left-most panel shows that for $m_b = 1.74$ and $N = 4$, most of the successful runs produced kinks with velocity ≈ 0.7 . As we decrease m_b , the velocity of the outgoing kinks decreases *e.g.* at $m_b = 1.47$, the peak occurs at $v_k \approx 0.6$. At $m_b = 1.12$, the success

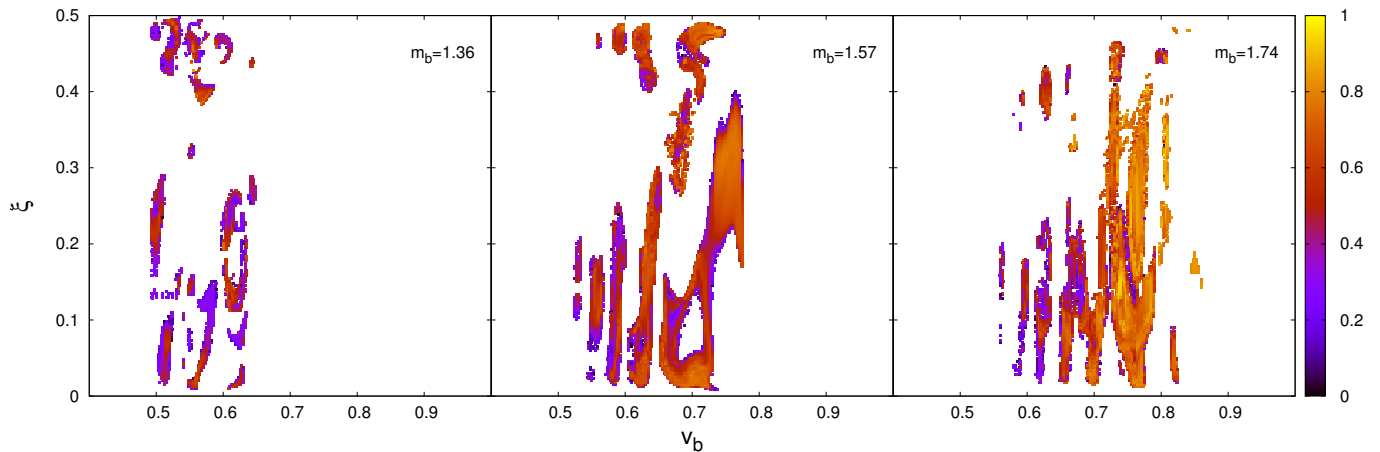


FIG. 4: Velocity of outgoing kinks (denoted by color) as a function of incoming breather velocity and twist for three breather masses. Band structure can be seen in the velocity dependence of successful production. The distinct drop in production for $\xi = 0.25 - 0.40$ can be observed for all masses. Further, we observe that lower values of m_b produce lower kink velocities.

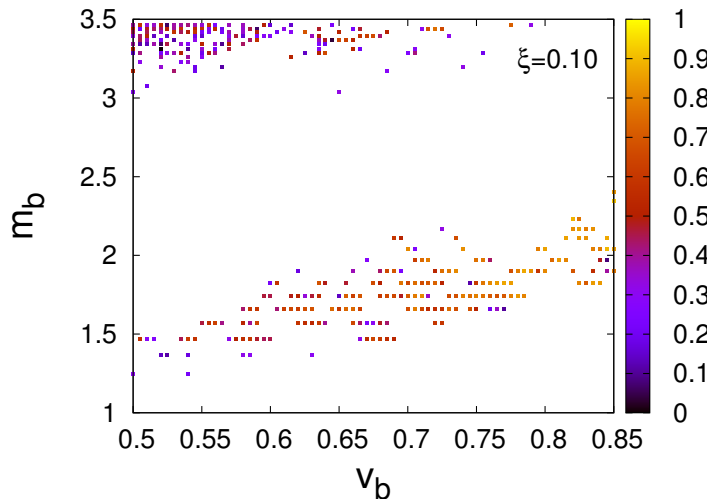


FIG. 5: v_k (denoted by color) is plotted vs v_b and m_b for $\xi = 0.10$. Successful kink production occurs in two bands that are well separated.

rate for kink productions very low and the outgoing kink velocity has decreased to ≈ 0.3 . Similarly, the center and right-hand panels of Fig. 6 show the dependence of v_k on v_b and ξ .

The trends in Fig. 6 can be quantified, as in Fig. 7, where we show how the mean value of v_k depends on m_b , v_b , and ξ . Linear fits give

$$\langle v_k \rangle_{v_b, \xi} = (0.56 \pm 0.04)m_b + (-0.34 \pm 0.05) \quad (22)$$

$$\langle v_k \rangle_{m_b, \xi} = (1.12 \pm 0.04)v_b + (-0.20 \pm 0.03) \quad (23)$$

where the subscripts refer to the parameters over which the data is accumulated. If we choose parameters such that the mean v_k is very small, it implies that any kink-antikink pairs that are produced will re-annihilate. Extrapolation from the above fits then suggests that kink production will be suppressed for $m_b < 0.6 \pm 0.1$ and $v_b < 0.18 \pm 0.03$. As a function of ξ we see that v_k doesn't seem to vary dramatically, but we do note a slight increase in v_k for $\xi = 0.25 - 0.35$.

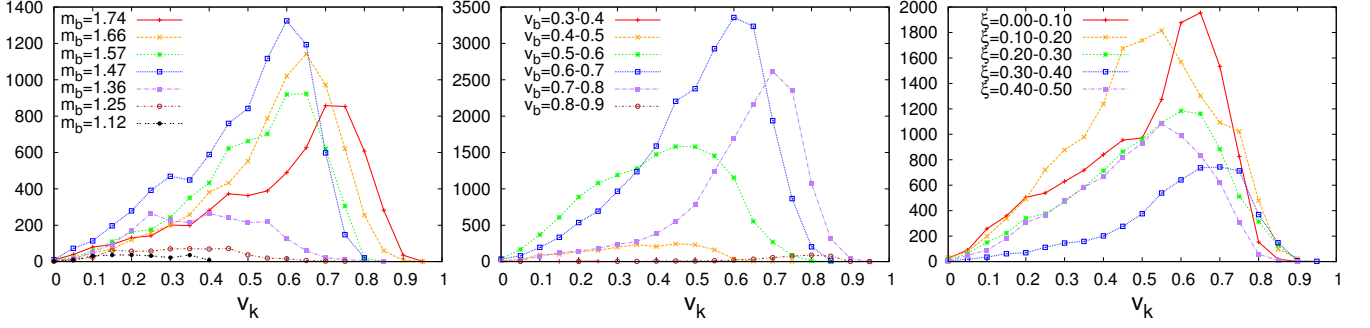


FIG. 6: Cumulative number of kink production events produced with velocity v_k from the set of initial conditions $m_b \in (1.12, 1.74)$, $v_b \in (0.0, 1.0)$, and $\xi \in (0.0, 0.5)$. In the left panel, successful events for all v_b and ξ are accumulated; similarly in the central panel, events for m_b and ξ are accumulated, and in the right panel, events for m_b and v_b are accumulated.

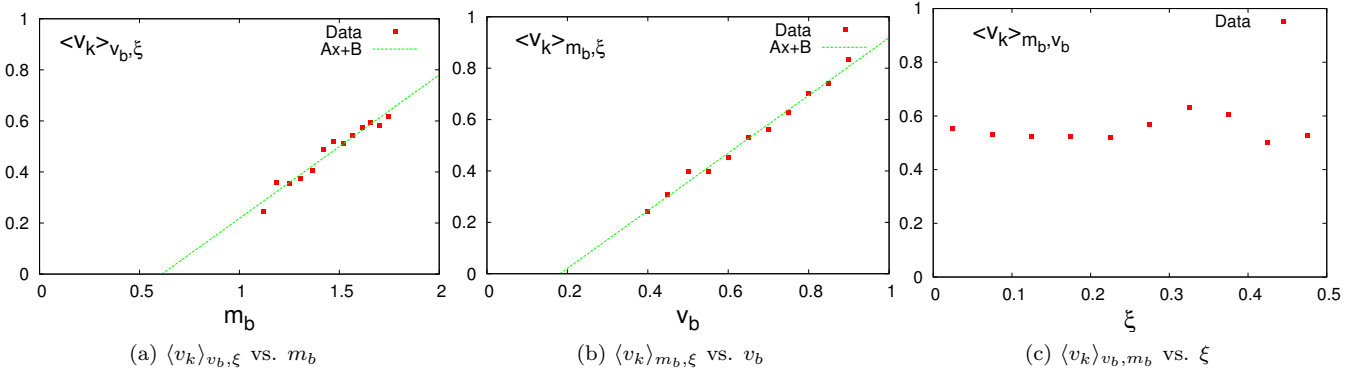


FIG. 7: Mean outgoing kink velocity as a function of initial conditions. In each of these plots, two of the three initial parameters, m_b , v_b , ξ are summed over.

A. Chaotic structure

One way to quantify the chaotic nature of conditions is to consider the fractal dimension of plots of the outgoing kink velocities, v_k , as a function of the initial conditions as shown in Fig. 4. Following the ideas of [11], we investigate a specific type of fractal dimension, the Minkowski-Bouligand dimension or the box-counting dimension. This dimension is defined by

$$D_{\text{box}} = \lim_{r \rightarrow 0} \frac{\log n(r)}{\log 1/r} \quad (24)$$

where $n(r)$ is the number of boxes of side length r that are required to cover the outline of the shape considered. For a shape lacking fractal properties in 2D (*e.g.* a circle) we get $D_{\text{box}} = 1$; while an area filling shape (*e.g.* a disc) has $D_{\text{box}} = 2$. A fractal shape in 2D has $1 < D_{\text{box}} \leq 2$. While Eq. (24) is the formal definition of the box-counting dimension, in practice it can be difficult to extract from data. Instead, since we expect the scaling of the boxes with r to be of the form

$$k(1/r)^{D_L} = n(r) \quad (25)$$

where D_L is called the local dimension and has a weak dependence on the box size for small r . Rearranging this equation we see that

$$-D_L \log(r) + \log(k) = \log(n(r)) \quad (26)$$

So the local dimension will be given by

$$D_L = -\frac{d \log(n(r))}{d \log(r)} \quad (27)$$

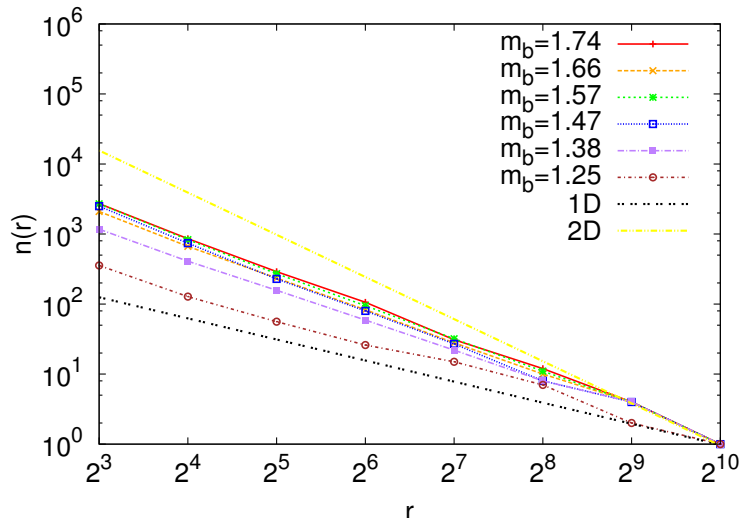


FIG. 8: Number of boxes required to bound the area of successful kink production as a function of the box side length for various breather masses. r is given in units of pixels. The plot begins at $r = 2^3$ because a point in our data corresponds to a 5×5 pixel box.

TABLE II: Mean value and standard deviation of the mean for the box counting fractal dimension, D_{box} , as a function of breather mass, m_b . We note that this is in general smaller than a similar value (1.770 ± 0.011) for the $\lambda\phi^4$ model found in [11]

m_b	D_{box}
1.74	1.58 ± 0.03
1.66	1.54 ± 0.04
1.57	1.60 ± 0.04
1.47	1.62 ± 0.06
1.38	1.42 ± 0.05
1.25	1.23 ± 0.10

and should be approximately D_{box} for small r . In Fig. 8 we plot the number of boxes needed to bound the area in Fig. 4 as a function of the side length. We have found that for increasing m_b there is a marked deviation from $D_{\text{box}} = 1$.

We compute D_L at each box size by taking 2nd order central finite differences and, for averaging over all r values, we arrive at a good estimate of box counting dimension, D_{box} . The results for D_{box} are shown in Table II for several m_b .

B. Dependence on Breather Mass

We expect that it is more difficult to produce kinks with low mass breathers than it is with high mass breathers. This expectation is seen to be correct in Fig. 9. We see that the success rate fluctuates around some value for $m_b > 2$, where we note that the kink energy is $E_k = 2$. While for $m_b < 2$, the success rate decreases exponentially with decreasing m_b . In the right panel of Fig. 9, we searched the $m_b < 2$ region more densely and fit the drop off with exponential and Gaussian profiles, with the Gaussian being marginally better in the low mass region.

Focusing on the low mass region of Fig. 9, we see that the lowest mass at which soliton production is achieved is $m_b = 0.9$. Due to the exponential fall-off at small breather mass, it would be very difficult to produce kinks using breathers of yet lower mass and a random choice for the other parameters.

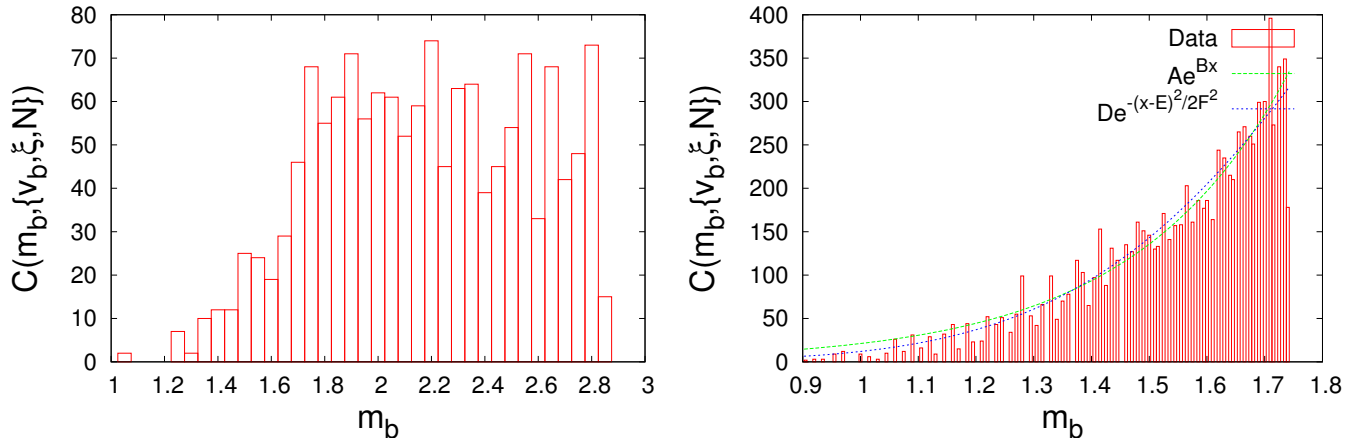


FIG. 9: Left: Accumulated number of successful events as a function of m_b over the range $m_b \in (1, 3)$ for all v_b, ξ and $N \in (2, 15)$. Right: A denser search over the range $m_b \in (0.9, 1.8)$ for all v_b, ξ and $N = 4$

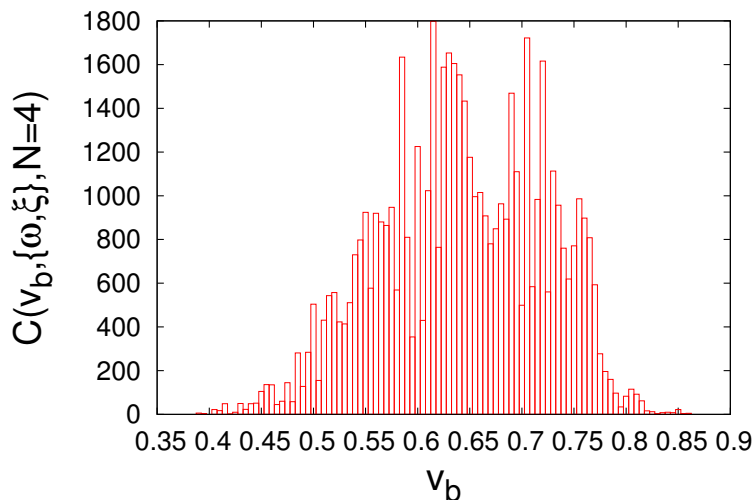


FIG. 10: Accumulated number of successful events as a function of v_b over the range $m_b \in (0.9, 1.8)$ for all m_b, ξ and $N = 4$

C. Dependence on Incoming Breather Velocity

Another important parameter for soliton production is the initial breather velocity. From Fig. 4 we see that kink production occurs when the incoming breather velocities lie in certain bands. These bands are insensitive to the breather mass and survive even after we sum over all m_b and ξ as seen in Fig. 10 where distinct peaks are present.

From our simulations, for a fixed breather mass, it is possible to calculate a mean breather velocity, $\langle v_b \rangle_\xi$, at which kink production is most likely. This value is found by accumulating the data from successful kink production over all twists and then finding the average breather velocity. The data is plotted in Fig. 11. The dependence of $\langle v_b \rangle_\xi$ on m_b is found to be linear in the region of $1.2 < m_b < 2$ with a fit

$$\langle v_b \rangle_\xi = (0.43 \pm 0.02)m_b + (-0.04 \pm 0.02) \quad (28)$$

Extrapolating to low mass, we obtain a mass cutoff at $m_b = 0.09 \pm 0.05$. This bound is much lower, hence weaker, than the bound of $m_b = 0.6$ obtained by requiring that the outgoing kinks have a non-zero velocity (see above Eq. 22).

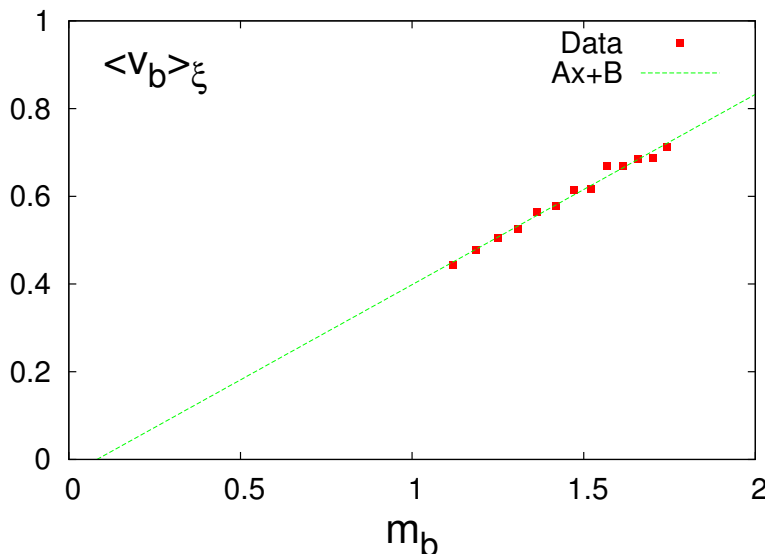


FIG. 11: $\langle v_b \rangle_\xi$ vs. m_b for $N = 4$. From the fit, we see that at $m_b = 0.09 \pm 0.05$, $\langle v_b \rangle_\xi \rightarrow 0$ which suggests that kink production with such low mass breathers is highly suppressed.

We therefore see that for breathers of lower mass to produce kinks, the velocity at which they must be collided is lower. But with lower breather velocity, the outgoing kink velocity also decreases, and at some point the kinks cannot escape and instead they re-annihilate. These results together indicate that kink production will be highly suppressed in low m_b regions in the (m_b, v_b) parameter space.

D. Dependence on Twist

An intuitive understanding of how the success of production should depend upon ξ is not obvious, but a few simple characteristics are expected. For $\xi = 0, 0.5$, the dynamics is the same as in the sine-Gordon model and we therefore expect there to be no kink production at these points. From Fig. 12, we see that this is in fact true. In the same figure, we see that even for small deviations from the sine-Gordon model, the production rate is quite large.

In previous sections, it has been seen that in a region located around $\xi = 0.25 - 0.40$ various interesting features occur. We have shown that the likelihood of production is decreased in this region (Fig. 4) and that the average outgoing kink velocity is slightly increased (Fig. 7). From Fig. 12 we see that the production count decrease in this region is over 40%, indicating some interesting physics must be occurring.

To understand the strange effects observed at $\xi = 0.25 - 0.40$ on twist, we investigated the case of two breathers whose centers of energy are initially at rest. Previous calculations have found that the force between two breathers in the sine-Gordon model is to first order [21]

$$F = \mp 16\eta^4 \omega^2 e^{-2\eta\omega|L|} \quad (29)$$

where the negative (positive) sign indicates attraction (repulsion) for in-phase (out-of-phase) breathers, and L is half the distance between the breathers. Since the phase of the breathers also corresponds to $\xi = 0$ for in-phase breathers and $\xi = 0.5$ for out-of-phase breathers, we expect that the force should be attractive for low twist, and repulsive for high twist in the $O(3)_z$ breather case. In [9], the time delay was numerically investigated for the $O(3)_z$ model and it was found that for $\xi = 0.2 - 0.4$ there was dramatic increase in time delay over the $\xi = 0, 0.5$ cases. Both of these works seem to indicate that at intermediate values of ξ there is something different about the breather interactions.

We have studied the dynamics of two initially static breathers for two different values of m_b and for various values of ξ . The results in Fig. 13 show that there is a critical value of twist at which the force changes from being attractive to being repulsive. The critical value depends on m_b and is larger for lower mass breathers. This suggests that the observed drop in kink production around $\xi \approx 0.3$ might be correlated with the lack of interaction between breathers at the critical twist.

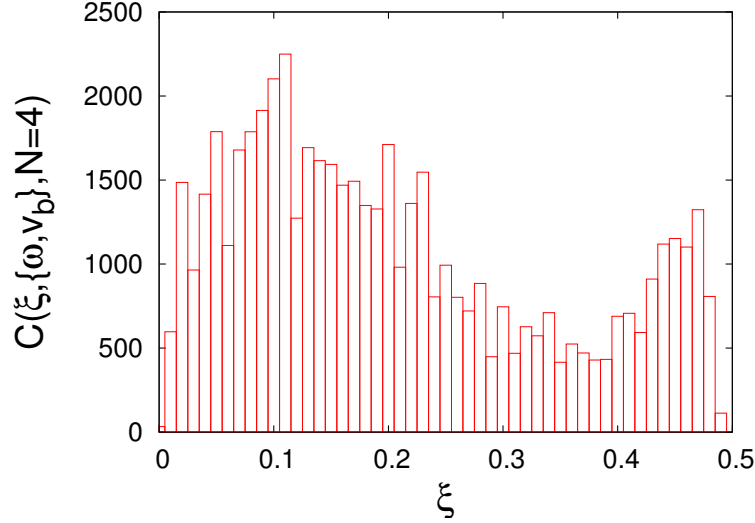


FIG. 12: Number of kinks produced vs ξ , summed over v_b , m_b and for $N = 4$. Notice that for $\xi = 0.25 - 0.4$ there is a distinct drop in production

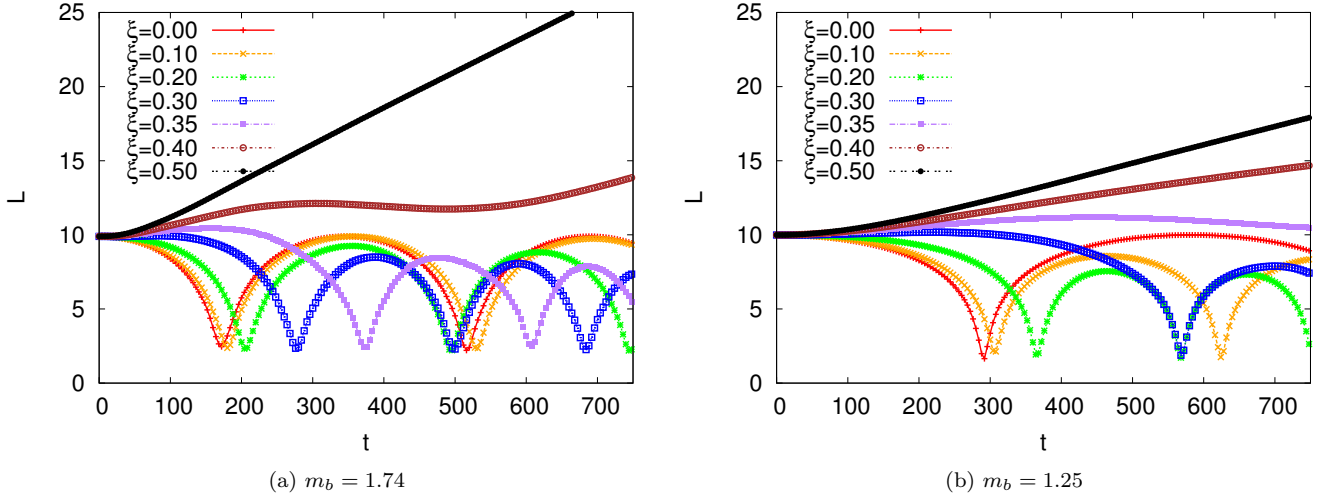


FIG. 13: Time evolution of the separation distance between two breather center of energies for $\xi = 0, 0.10, 0.20, 0.30, 0.35, 0.40, 0.50$ for $m_b = 1.74, 1.25$. Below a critical value of $\xi \approx 0.35 - 0.40$ the force is attractive and the breathers oscillate about a shared center; above the critical value, the breathers repel and move apart.

E. Dependence on Number of Breathers

As one might expect, increasing the number of breathers in the initial train of breathers increases the chances of kink production. This data is shown in Fig. 14. The shown fit corresponds to logarithmic growth of successful kink production events with the number of breathers. So the gain in kink production depends weakly on the number of breathers. This agrees with our earlier discussion in the context of the left panel of Fig. 3, where we suggested that it is the energy per breather that is important for kink production and not so much the total energy in the train of breathers.

To further understand the effects of N , we investigated a set of initial conditions where for $N = 4$ we know solitons are produced, and then we varied N . We found, as seen in Fig. 2, that the solitons were produced in the collision

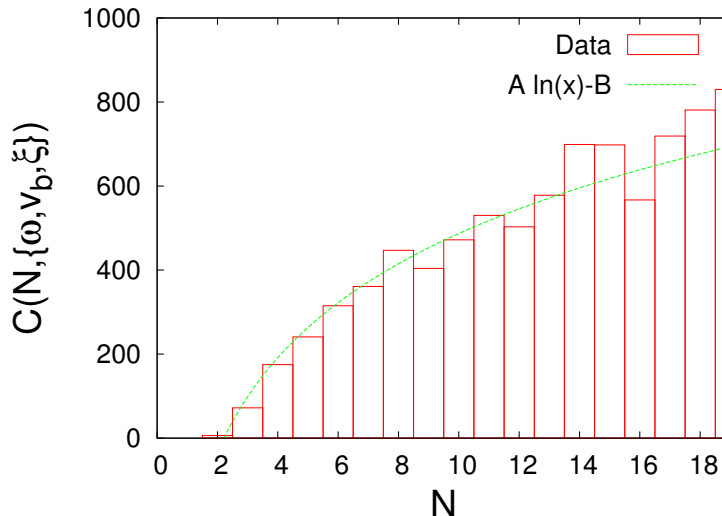


FIG. 14: Number of kinks produced vs. N , summed over v_b , m_b and ξ . The likelihood of kink production increases, but slows with increasing N . A good fit was found to be $(330 \pm 30) \ln(N) - (280 \pm 70)$.

of the second breathers in each train before the third and fourth had had a chance to collide. This result is at first troubling because for the cases of $N = 1, 2, 3$ it is found that no kinks are produced. So the fourth breather in the train is critical to kink production. The exact role that the fourth breather plays is not clear to us though some possibilities come to mind. The fourth breather may influence the forward breathers in the train prior to the collision and change some of their characteristics, and this is what enables kink production. Another possibility is that the collisions of the number two breathers produce a proto-kink pair which requires additional momentum transfer via the fourth breather to grow into a kink-antikink pair.

We speculate that the diminishing return on success of additional breathers arises from the limitation imposed on interaction between breathers based on their initial spacing in the trains. Although the numbers of breathers increases, the distance between the beginning and end of the train also increases. Since the force between breathers is generically exponential with distance (i.e. Eq. 15), breathers that are sufficiently far away have little effect on each other.

F. Other Initial Conditions

In Sec. III, it was discussed that there is a freedom in choosing $\dot{\phi}(t = 0)$. In the previous discussions we have only studied the simplest case of $\dot{\phi}(t = 0) = 0$. Here we consider two other possible set of initial conditions. The first type is the “co-spinning” initial conditions

$$\dot{\phi}(t = 0, x) = v_\phi \quad (30)$$

where v_ϕ is some constant velocity and all the breather trains rotate have the same velocity in the ϕ variable. Additionally, we considered “counter-spinning” initial conditions

$$\dot{\phi}(t = 0, x) = v_\phi \tanh(x/w) \quad (31)$$

where the left-moving and right-moving breather trains have opposite velocity in the ϕ direction. These choices both introduce another free parameter into the initial conditions, namely, the initial ϕ velocity v_ϕ . On inclusion of a $\dot{\phi}$ term into the equations of motion, the sine-Gordon breathers are no longer exact solutions, but from our simulations they are found to still be long-lived.

Spinning initial conditions may also be viewed as charged initial conditions, following the remark below Eq. (4). Co-spinning initial conditions correspond to like charges on the incoming breather trains; counter-spinning initial conditions correspond to opposite charges on the breather trains.

We have run our simulations for the co-spinning and counter-spinning initial conditions with $v_\phi = 0.1$, $m_b = 1.36$, and $N = 4$ and some of the results are shown in Fig. 15. The co-spinning initial conditions have only 80% of the

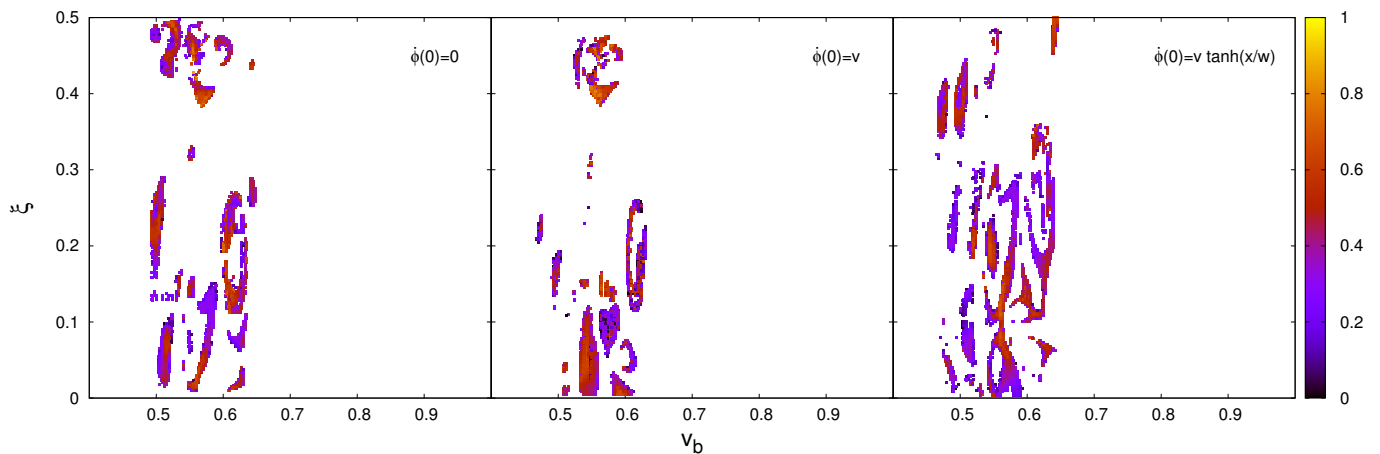


FIG. 15: Velocity of outgoing kinks (denoted by color) as a function of incoming breather velocity and twist for the non-spinning (left panel), co-spinning (center panel), and counter-spinning (right panel) initial conditions for $m_b = 1.36$, $v = 0.1$, and $N = 4$.

number of successful kink production events as the non-spinning initial conditions for the same phase space search. Furthermore, the distributions in breather velocity and twist are shifted to lower values and have smaller spreads. The mean outgoing kink velocity is also decreased. Putting these trends together, we conjecture that co-spinning initial conditions suppress kink production, but additional study should be undertaken to confirm this.

Counter-spinning initial conditions appear to have exactly the opposite effects. The spread in breather velocities and twist increased, and the final kink velocities also increased. For the same parameter space search, counter-spinning runs were more successful than non-spinning runs by a factor of 1.4, suggesting that such initial conditions may be worth exploring further.

V. CONCLUSIONS

We have numerically explored a wide range of scattering initial conditions in the $O(3)_z$ model that can lead to the production of a kink-antikink pair. Our initial state consists of two oppositely moving trains of breather solutions. There are several general features that we have observed that we now summarize: (i) the region in parameter space that leads to kink production has fractal structure, (ii) smaller breathers need to be scattered at smaller velocities, (iii) when kinks are produced, their outgoing velocities increase in proportion to the incoming breather train velocity, (iv) twist is essential for kink production in this model but the outcomes are not strongly sensitive to the exact value that we choose, and (v) the force between breathers vanishes for a certain value of the twist. Putting together points (ii) and (iii) we conclude that small breather velocities are necessary for building kinks, while large breather velocities help to separate them. Hence there is tension in the requirements for successful kink production and we can expect that the process will be highly suppressed when the breather mass is small compared to the kink mass.

These pessimistic conclusions are somewhat offset by our finding that counter-spinning initial conditions can enhance kink production. Further exploration of such initial conditions may lead to better understanding of when kinks can be (more easily) produced.

Finally we observe that, since the sine-Gordon model is embedded inside the $O(3)_z$ model, and soliton operators have been constructed in the sine-Gordon model [22], it is possible that similar operators can be found in the quantum $O(3)_z$ model. Then it is conceivable that kink production can be studied in the $O(3)_z$ model by quantum field theory methods or on a lattice.

Acknowledgments

The numerical work was done on the Saguario cluster at the ASU Advanced Computing Center. This work was supported by the DOE at ASU.

-
- [1] E. Mottola and A. Wipf, *Phys.Rev.* **D39**, 588 (1989)
 - [2] A. Ringwald, *Nucl.Phys.* **B330**, 1 (1990)
 - [3] M. P. Mattis, *Phys.Rept.* **214**, 159 (1992)
 - [4] C. Rebbi and J. Singleton, Robert L., *Phys.Rev.* **D54**, 1020 (1996), arXiv:hep-ph/9601260 [hep-ph]
 - [5] A. Kuznetsov and P. Tinyakov, *Phys.Rev.* **D56**, 1156 (1997), arXiv:hep-ph/9703256 [hep-ph]
 - [6] F. Bezrukov, D. Levkov, C. Rebbi, V. Rubakov, and P. Tinyakov, *Phys.Rev.* **D68**, 036005 (2003), arXiv:hep-ph/0304180 [hep-ph]
 - [7] D. Levkov and S. Sibiryakov, *Phys.Rev.* **D71**, 025001 (2005), arXiv:hep-th/0410198 [hep-th]
 - [8] S. Demidov and D. Levkov, *Phys.Rev.Lett.* **107**, 071601 (2011), arXiv:1103.0013 [hep-th]
 - [9] T. Vachaspati, *Phys.Rev.* **D84**, 125003 (2011), arXiv:1109.1065 [hep-th]
 - [10] S. Dutta, D. A. Steer, and T. Vachaspati, *Phys.Rev.Lett.* **101**, 121601 (2008), arXiv:0803.0670 [hep-th]
 - [11] T. Romanczukiewicz and Y. Shnir, *Phys.Rev.Lett.* **105**, 081601 (2010), arXiv:1002.4484 [hep-th]
 - [12] S. Demidov and D. Levkov, *JHEP* **1106**, 016 (2011), arXiv:1103.2133 [hep-th]
 - [13] P. Anninos, S. Oliveira, and R. Matzner, *Phys.Rev.* **D44**, 1147 (1991)
 - [14] D. K. Campbell, J. F. Schonfeld, and C. A. Wingate, *Physica* **9D**, 1 (1983)
 - [15] A. B. Zamolodchikov and A. B. Zamolodchikov, *Annals Phys.* **120**, 253 (1979)
 - [16] T. Vachaspati, *Kinks and domain walls: An introduction to classical and quantum solitons* (2006)
 - [17] R. F. Dashen, B. Hasslacher, and A. Neveu, *Phys.Rev.* **D11**, 3424 (1975)
 - [18] S. A. Teukolsky, *Phys.Rev.* **D61**, 087501 (2000), arXiv:gr-qc/9909026 [gr-qc]
 - [19] F. Feroz, M. Hobson, and M. Bridges, *Mon.Not.Roy.Astron.Soc.* **398**, 1601 (2009), arXiv:0809.3437 [astro-ph]
 - [20] F. Feroz and M. Hobson, *Mon.Not.Roy.Astron.Soc.* **384**, 449 (2008), arXiv:0704.3704 [astro-ph]
 - [21] M. Nishida, Y. Furukawa, T. Fujii, and N. Hatakenaka, *Phys. Rev. E* **80**, 036603 (Sep 2009), <http://link.aps.org/doi/10.1103/PhysRevE.80.036603>
 - [22] S. Mandelstam, *Phys.Rev.* **D11**, 3026 (1975)